

Follow Anything: Open-set detection, tracking, and following in real-time

Alaa Maalouf^{1,*}, Ninad Jadhav², Krishna Murthy Jatavallabhula¹, Makram Chahine¹,
Daniel M. Vogt², Robert J. Wood², Antonio Torralba¹, and Daniela Rus¹

¹CSAIL, MIT ²SEAS, Harvard University *Correspondence: alaam@mit.edu

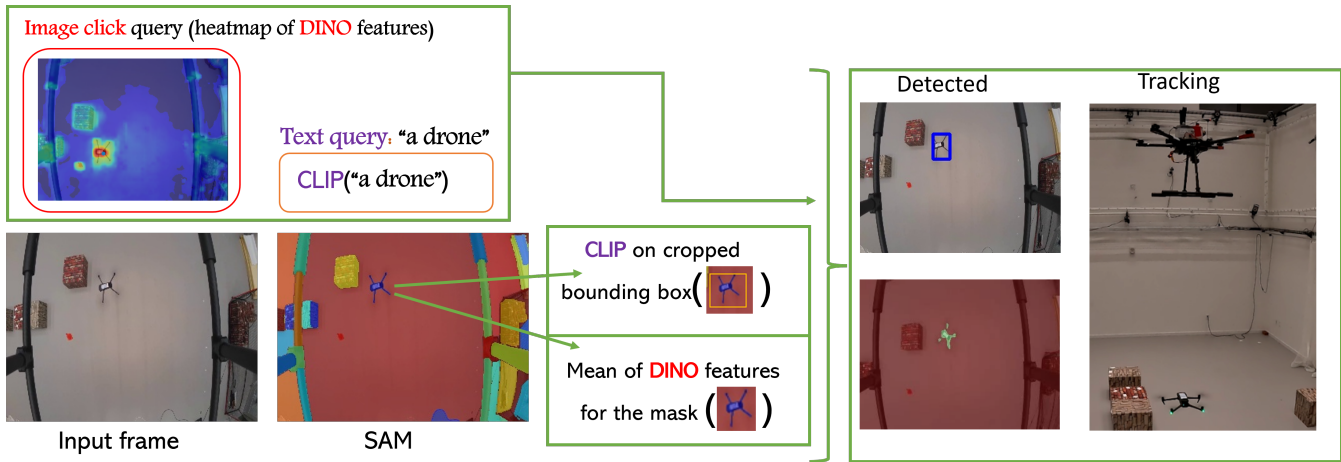


Fig. 1: **Follow anything** (*FAn*) is a real-time robotic system to detect, track, and follow objects in an open-vocabulary setting. Objects of interest may be specified using text descriptions, images, or clicks. *FAn* then leverages foundation models like CLIP [1], DINO [2], and SAM [3] to compute segmentation masks and bounding boxes that best align with the queried objects. These objects are tracked across video frames, accounting for occlusion and object re-emergence; enabling real-time following of objects of interest by a robot platform. On the right, we show *FAn* being deployed on a micro aerial vehicle (MAV), following an object of interest (here, another smaller *drone*). *FAn* can be deployed on a commodity laptop with a lightweight (6-8 GB) GPU, achieving real-time (6-20 fps) throughput. We encourage the reader to view the demos on our [project webpage](#) and check the [explainer video](#).

Abstract—Tracking and following objects of interest is critical to several robotics use cases, ranging from industrial automation to logistics and warehousing, to healthcare and security. In this paper, we present a robotic system to detect, track, and follow any object in real-time. Our approach, dubbed *follow anything* (*FAn*), is an open-vocabulary and multimodal model – it is not restricted to concepts seen at training time and can be applied to novel classes at inference time using text, images, or click queries. Leveraging rich visual descriptors from large-scale pre-trained models (*foundation models*), *FAn* can detect and segment objects by matching multimodal queries (text, images, clicks) against an input image sequence. These detected and segmented objects are tracked across image frames, all while accounting for occlusion and object re-emergence. We demonstrate *FAn* on a real-world robotic system (a micro aerial vehicle), and report its ability to seamlessly follow the objects of interest in a real-time control loop. *FAn* can be deployed on a laptop with a lightweight (6-8 GB) graphics card, achieving a throughput of 6-20 frames per second. To enable rapid adoption, deployment, and extensibility, we open-source all our code on our project webpage: <https://github.com/alaamaalouf/FollowAnything>. We also encourage the reader to watch our 5-minutes [explainer video](#).

I. INTRODUCTION

Detecting, tracking, and following objects of interest is critical to several robotics use-cases, such as industrial automation, logistics and warehousing, healthcare, and security [4]–[8]. Notably, one of the key drivers of continuous progress in providing robust object-following systems is the combination of computer vision and deep learning [5], [9], [10], where training deep convolutional networks on large labeled datasets have made tremendous strides in this area. However, existing robotic systems for object following suffer two notable shortcomings:

- 1) They are *closed-set*, i.e., the set of objects to detect and follow is assumed to be available a priori (during the training phase). This means such systems are only able to handle a *fixed set of object categories* [5], [11]–[14], limiting their adaptability; adapting to newer object categories necessitates finetuning the model.
- 2) Additionally, the objects of interest are specified (queried) only by a class label, which is *often unintuitive for end-users* to specify, imposing restrictions on how users interact with the system [5], [15], [16].

Deep learning approaches are currently undergoing an-

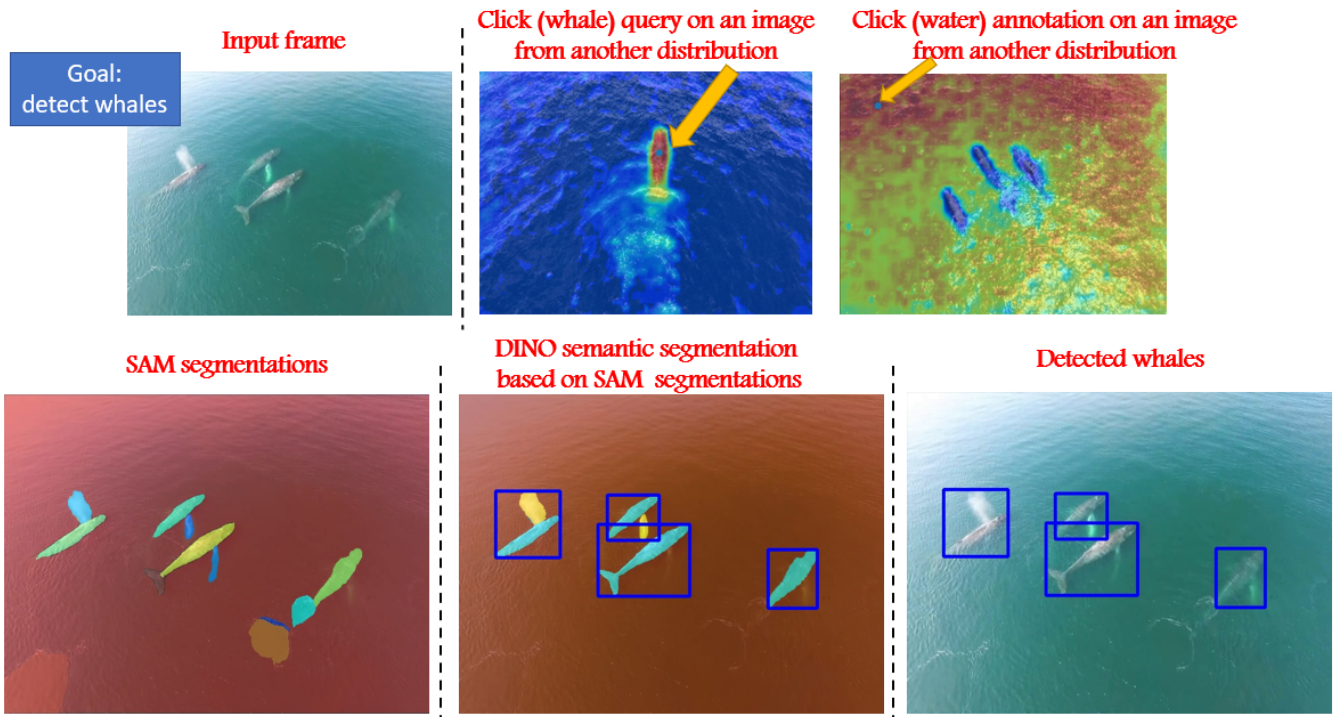


Fig. 2: *FAn* outputs illustrations on input frame of 4 whales with a click query on a whale and click query on water. In the first step, SAM extracts multiple masks (segmentations), then, based on DINO features, *FAn* classifies each mask to what object it refers from the given queries (water/whales). Finally, whales are detected by assigning the masks whose DINO feature descriptor is closest to the whales’ query feature descriptor. NOTE: The heat maps are shown in the click (query) figures.

other wave of ever-more performant and robust model design, with the creation of increasingly big and multimodal models trained on internet scale amount data containing hundreds of millions of images, text, and audio. These highly capable models (e.g., CLIP [1], DINO [2]) have demonstrated impressive performance in open-set scenarios (i.e., the objects of interest are only supplied at inference time, and not trained for a specific task) [17], [18]. Notably, recent robotics approaches using foundation models have shown impressive open-set interaction abilities [19]–[23], and extended robustly to multimodal applications [24]–[27]. However, integrating these performant neural network architectures into real-time and resource-constrained robotic systems poses significant challenges, due to their large model size and high inference latency.

A. Our Contributions

We address the pre-discussed gaps by developing an *open-set* real-time any object following approach, which can flexibly adapt to categories specified at inference time, via multiple modalities including text, images, and clicks. Specifically, we bring together recent advances in vision and vision-language foundation models and present the *follow anything* system (*FAn*), which is

- an **open-set, multimodal** approach to detect, segment, track, and follow *any* object in **real-time**. The object of interest may be specified via an input text prompt, an image, a bounding box, or a click.

- a *unified* system that is easily deployed on a robot platform (in our work, a micro aerial vehicle). The system includes real-time processors for input image streams and visual-servoing control loops for following the object of interest.
- built with *re-detection mechanisms* that account for scenarios where the object of interest is occluded or tracking is lost. This mechanism can function autonomously or with human guidance, ensuring the object is successfully identified and tracked again, maintaining continuity in the tracking process.

We experimentally validate our system by autonomously detecting, tracking, and following a multitude of mobile agents including a drone, an RC car, and a manually operated brick.

II. OUR APPROACH: *FAn*

Open-vocabulary object following: Given (1) a robotic system (here, a micro aerial vehicle) equipped with an onboard camera, and (2) an object of interest within the onboard camera’s field-of-view (specified either as a text prompt, an image, a bounding box, or a click); the object following task involves detecting the object of interest, and producing robot controls u_t at each time step t such that the object of interest is constrained to always completely be within the field of view of the onboard camera.

This is an extremely challenging task; it necessitates correctly identifying the object of interest and determining its position relative to the robot’s onboard camera frame,

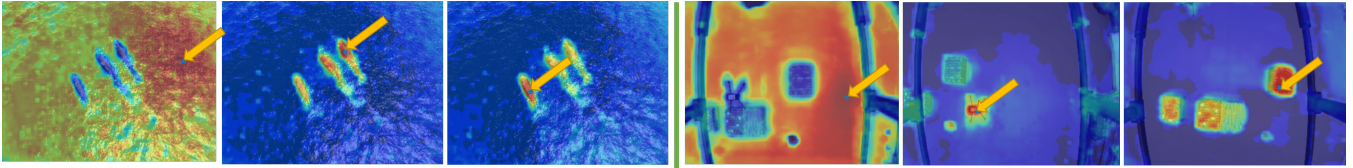


Fig. 3: Heat maps showing the pixels’ semantic similarity for high and low-resolution images. For every pixel, its feature descriptor is extracted then cosine similarity is computed between its descriptor and a focal point pixel descriptor (pointed at by a yellow arrow).

all the while accounting for variations in the environment, background clutter, object size, etc. It also then requires the object of interest to be continuously tracked across time; while at the same time, the robot controller needs to output a sequence of stable velocities (or accelerations) and simultaneously ensure the stability of the robot and the visibility of the tracked object.

FAn system overview: *FAn* uses a combination of state-of-the-art ViT models, optimizes them for real-time performance, and unifies them into a single system. In particular, we leverage the segment anything model (SAM) [3] for segmentation, DINO [2], and CLIP [1] for general-purpose visual features, and design a lightweight detection and semantic segmentation scheme by combining the features from CLIP and DINO with the class-agnostic instance segmentation determined by SAM. We use the (Seg)AOT [28], [29] and SiamMask [30] models for real-time tracking, and design a lightweight visual servoing controller for object following.

A. Real-time Open-vocabulary Object Detection

We first describe our lightweight object detection and segmentation pipeline that builds atop SAM, CLIP, and DINO. Our system takes as input an RGB frame from a video stream, represented by a 3D tensor $F \in \mathbb{R}^{h \times w \times 3}$, and a query q representing the desired object to detect in the video, (e.g., a text “a blue whale”, an image of a whale, or a click on a whale from another image). The object detection subsystem is tasked to detect the object specified by the user query q in an input image frame.

We use *Seg* to denote the class-agnostic instance segmentation operator (SAM [3] or Mask2Former [31]). *Seg* takes as an input the current frame F , and outputs a set of n masks $\{M_1, \dots, M_n\} := \text{Seg}(F)$ (n depends on the input frame and is not a constant), where each mask $M_i \in \mathbb{R}^{h \times w}$ is a binary matrix with ones in the indices of pixels defining the corresponding segmented object, and zeros elsewhere. We also use *Desc* to denote a feature extractor model; which in our case is either the DINO or CLIP vision transformer (ViT) model. These models extract pixel-wise feature descriptors using techniques described e.g., in [32], [33] and summarized in Section II-C. *Desc* receives as an input the current frame F , and outputs a descriptor tensor $D := \text{Desc}(F) \in \mathbb{R}^{h \times w \times d}$, where for every pixel in F , a descriptor vector of dimension d is constructed. This d dimensional vector encapsulates the semantic information about its corresponding pixel. Additionally, *Desc* can be also used to provide a feature descriptor $v := \text{Desc}(q) \in \mathbb{R}^d$ for the input query q .

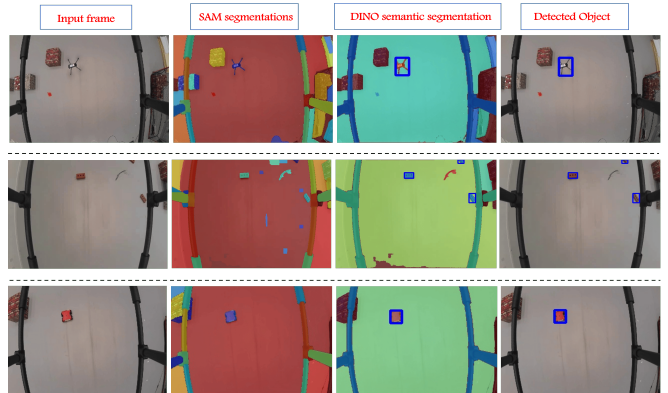


Fig. 4: **Automatic detection experiments (SAM-and-DINO).** Examples of our automatic detection scheme for detecting Drones, Bricks, and RC Cars. The examples include (from left to right): the original input frame, the outputs of SAM segmentation masks, and DINO+Cosine similarity semantic segmentation and detection.

Embedding input queries. To detect the desired object referred to by the query q , we start by computing the feature descriptor of the query q : $v := \text{Desc}(q)$, such that v encodes the information in the feature space representing the object described by the query q . Now the system starts receiving frames from the stream, and for every frame F_i ($i := 1, 2, 3 \dots$), *FAn* applies the following steps.

First, we compute the (binary) instance segmentation masks by applying *Seg* on F_i , $\{M_1, \dots, M_n\}_i := \text{Seg}(F_i)$. Intuitively, this step partitions the frame into n objects (regions) and a background, however, none of these objects are classified as labeled/identified objects. Additionally, these regions might intersect. Hence, what is missing, is to predict for each region, whether it is the desired object to track or not. In the case where a set of queries $Q = \{q_1, \dots, q_m\}$ is given, the goal is to classify which query amongst the m provided matches (if any) best each segment $M_j \in \text{Seg}(F_i)$. This brings us to the second step.

Second, we extract the pixel-wise descriptors by applying *Desc* on F_i , $D_i := \text{Desc}(F_i) \in \mathbb{R}^{h \times w \times d}$. After this step, D_i contains $h \cdot w$ descriptors, where each descriptor corresponds to a pixel in the input image. To compare each region (mask) with the given input query q , we need to aggregate these per-pixel descriptors to form region-level descriptors. We find the average pooling aggregation operator to be fast and effective for this purpose. This not only provides us with a more generic descriptor encapsulating all of the features across the specific mask, but also improves the performance of the downstream system modules. Opposed to comparing the q



Fig. 5: **Fast automatic detection experiments (DINO only):** Examples of our fast automatic detection scheme on detecting (1) whales, (2) drones, (3) RC cars, and (4) toy bricks. Although this approach is much faster and works well for objects with unique shapes like drones and whales, it provides a less "clean" segmentation, resulting in higher chances of miss-detection, specifically, for objects of non-unique shapes as the brick in the last column.

query’s feature descriptor v to all of the per-pixel descriptors associated with a specific mask, we only need to compare the aggregate region-level descriptors. Thus, the next step in our pipeline involves computing the mean feature descriptor v_j for each segmentation region, i.e., for every $j \in \{1, \dots, n\}$:

$$v_j := \frac{1}{\text{non-zero}(M_j)} \sum_{p \in D_i[M_j]} p$$

where $\text{non-zero}(M)$ denotes the number of non-zero entries in binary matrix M , and $D_i[M_j]$ denotes the set of d dimensional vectors from D_i corresponding to the non-zero pixel entries in the mask M_j .

The vector v_j , encodes all of the semantic information representing the region of the segment M_j in the features space. Hence for every region (segment/mask) $j \in \{1, \dots, n\}$, we have its corresponding feature descriptor v_j .

Similarity scores: Given a query (in the form of text, image, or click), we first extract a query feature descriptor v by applying a modality-specific encoder (CLIP text encoder for text-query, DINO or CLIP image encoder followed by average pooling for image-query, directly selecting the closest pixel/patch feature for click-query). To match this query to the current image, we compute the cosine similarity between each region descriptor v_j , and the query feature descriptor v as:

$$\cos(v_j, v) := \frac{v_j^T v}{\|v_j\| \|v\| + \epsilon}$$

where $\epsilon > 0$ is a small constant, for numerical stability. This is the fourth step, and it intuitively measures how similar each mask (region) is to the query features descriptor.

Single query detection. If the similarity $\cos(v_j, v)$ between the given query and the mask feature descriptor is larger than a given threshold α , we assign the region corresponding to this mask in the original frame the label of the query.

Multi-class zero shot detection. Similarly to the case of a single query, should the user provide a set of queries $Q = \{q_1, \dots, q_m\}$, the system computes the feature descriptor $v^k := \text{Desc}(q_k)$ for every $q_k \in Q$, and then, for every pair of query feature descriptor $v^k \in Q$ and region descriptor vector v_j , it computes: $\cos(v_j, v^k)$. Now, for every $j \in \{1, \dots, n\}$, it finds its closest (most similar) query:

$$\max_{k \in \{1, \dots, m\}} \cos(v_j, v^k).$$

TABLE I: Runtime in frames per second (FPS) for all of the used models on an NVIDIA GeForce RTX 2070 on-board a laptop.

Model	FPS		Subtask
	frame size 320 × 240	frame size 640 × 480	
SAM (points.per.side = 16)	0.71	0.58	Segmentation
SAM 16BIT (points.per.side = 16)	0.97	0.71	
FASTSAM	10.7	10.2	
DINO	4.76	4.68	Feature extraction for click/image queries
DINO TRACED	6.27	NA	
DINO 16BIT	10.63	11.55	
DINO 16BIT+TRACED	17.46	17.44	
CLIP	7.81	7.65	Feature extraction for text queries
CLIP 16BIT	21.12	20.21	
SIAMMASK	50.3	49.2	Tracking
DEAOT	28.74	17.13	

Finally, when the cosine similarity between the query vector (denoted as v^k), and the mask feature descriptor (v_j), exceeds a specified threshold α , we assign the label of the query to the region in the original frame that corresponds to this mask, otherwise, it is considered "non-labeled".

After this process, each pixel is assigned a label from $\{1, \dots, m\}$, or 0 if unlabeled. Figure 2 provides an illustration of the whole detection flow, and Figures 4 and 8 present results on detecting objects via SAM+DINO, and SAM+CLIP respectively. For more experimental details, see Section III.

Bounding box query: We also provide an option for the user to manually draw bounding boxes (or provide outputs from a customized domain-specific detector) around the objects they wish to track, or alternatively, click on one or two pixels within the object (in real-time from the video stream). Once the user has made their selection, we employ SAM to segment and obtain the mask of the selected object. This process is accurate and reliable, making it ideal for scenarios where the user wants to be in complete control of the object-tracking process and needs a high degree of accuracy to ensure that the detection is indeed correct.

B. Fast Detection for Limited Hardware

Off-the-shelf implementations of foundation models like SAM and DINO are not well-suited for real-time onboard detection, segmentation, and tracking. SAM takes several seconds to compute segmentation masks per frame. While we evaluated the recently proposed FastSAM [34] model and obtained a $15\times$ speedup on our hardware with comparable performance, the best runtime achieved by FastSAM is between 10 and 12 FPS, which is still insufficient for detecting fast-moving objects. This is because segmentation outputs also need to be supplemented by features from ViT models, and the detection, tracking, and following submodules.

Fast detection by (solely) grouping DINO features: To mitigate this compute bottleneck, we instead propose to first obtain coarse detections by grouping DINO features. These coarse detections may further be refined by periodically computing segmentation masks and tracking these over time, effectively rendering the overall system operable at high frame rates. To obtain coarse detections, we (i) We extract the pixel-wise descriptors by applying Desc (DINO) on the current input frame F_i , $D_i := \text{Desc}(F_i) \in \mathbb{R}^{h \times w \times d}$, (ii) given the inputs set of queries $Q = \{q_1, \dots, q_m\}$, the system computes the cosine similarity $\cos(v_{h,w}, v^k)$ for each pair of query $q_k \in Q$ (where $v^k := \text{Desc}(q_k)$) and pixel-wise

TABLE II: Runtime in frames per second (FPS) for the detection phase of the system on an NVIDIA GeForce RTX 2070, compared to the popular open-source library [35], using a more powerful GPU of NVIDIA RTX 3090.

Approach	FPS	
	frame size 320 × 240	frame size 640 × 480
OURS WITH SAM	0.601	0.536
OURS WITH FASTSAM	9.153	9.172
OURS WITH JUST DINO (NO SAM OR FASTSAM)	15.67	14.37
GROUNDSED-SAM [35]	0.508	0.51

descriptor vector $v_{h,w}$. Next, as previously, (iii) for each pixel, it picks the closest (most similar) query, i.e., the one with the maximum cosine similarity. Now, (iv) if the cosine similarity between the query vector v^k and the pixel feature descriptor $v_{h,w}$ surpasses a specified threshold α , we assign the label of the query to the corresponding pixel in the original frame F_i . Otherwise, it is considered as "non-labeled". Finally, (v) one can apply "extract contours" to obtain the "desired" detected objects based on the semantic segmentation results. See Figure 5 for experiments that leverage the coarse detection module proposed here.

Optimizing DINO runtime: We speed up the DINO ViT models further by employing two model optimization techniques: quantization and tracing. Quantization reduces the precision of numerical values in the model (often by using fewer bits to encode model parameters), which decreases memory requirements and computational complexity. By representing values with fewer bits, inference time is shortened and hardware resource utilization is improved. Tracing, an alternative optimization technique, involves converting a dynamic computational graph into a static graph representation, enabling ahead-of-time optimizations and efficient parallelization. Together, quantization and tracing play a crucial role in enhancing the efficiency and speed of the DINO model while maintaining its overall accuracy and effectiveness; See Table I for runtime details of DINO, optimized DINO, and all of the other models used in the system. We report the running time for each model independently, not as part of the whole system. Note that some models automatically reshape inputs to a constant size. We also compare the runtime of our detection phase, with popular alternatives like Grounded-SAM [35] method in Table II.

C. Extracting per-pixel feature descriptors

While a few methods adapt foundation models like CLIP to provide per-pixel descriptors, these methods [36]–[39] require model re-training or finetuning on an image-text aligned dataset. This often results in concepts absent in the finetuning set being forgotten by the models, as demonstrated in ConceptFusion [33], where the adapted models particularly struggle with fine-grained concepts. To counteract this, [33] presents a zero-shot method for constructing pixel-aligned features that combine local (region-level) data with global (image-level) context included in models like CLIP. For efficiency (real-time processing) purposes, we adapt part of this method in our system when using CLIP for providing pixel-wise feature descriptors, however, we only use their

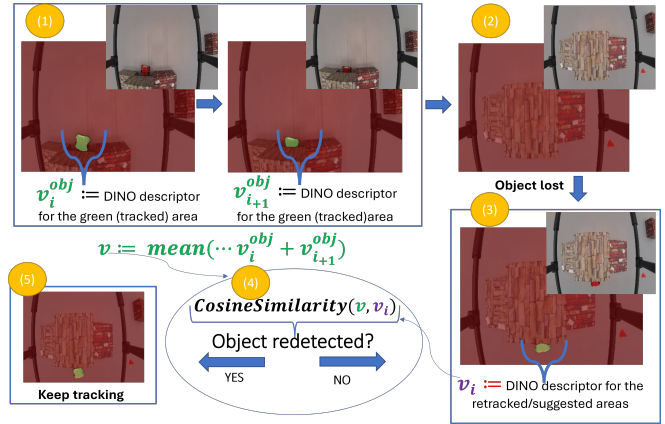


Fig. 6: **Automatic re-detection via cross trajectory stored ViT features.** (1) At every frame, we store the DINO features representing the tracked object. (2) Once the object is lost, we (3) either apply a segmentation model or get suggested masks from the tracker, for every mask, we compute the DINO descriptors, and (4) compare it to the pre-computed ones. If a high similarity is obtained we go to (5) and keep tracking the object, else, we apply step (3) again on the next frame.

ablated baseline which computes purely local 2D features by extracting a bounding box around each segmentation mask (obtained from FastSAM) and passes them through the CLIP image encoder. For DINO, we use [32] as is, and find that their pixel-wise feature descriptors are inherently informative. Our quantized and traced DINO model makes the feature extraction process much faster (17 fps) without losing accuracy.

D. Re-detecting a Lost Object

We also provide three flavors of re-detection mechanisms to address situations where the tracked object is temporarily lost. These mechanisms range from completely automated to human-in-the-loop re-detection approaches, and depending on the downstream application, a suitable technique may be adopted.

In the event of a temporary loss of the tracked object, either due to occlusion or abrupt motion, our system automatically initiates a re-detection process. Users have an option, before the FAn pipeline is launched, to select the level and nature of re-detection support needed. The first (and simplest) level waits until the tracker itself re-detects the object. Although this is the fastest technique, it lacks robustness and may sometimes falsely detect another object (of the same category) in the frame. The second approach offers a human-in-the-loop re-detection mechanism; the system reports that tracking is lost, and then a user performs a click of bounding box query. However, this assumes a human operator is available and alert. While this is the case in safety critical applications, this is not always feasible. To mitigate this, we also propose an automatic re-detection technique.

Automatic re-detection via cross trajectory stored ViT features. To enable a robust and accurate autonomous re-detection of the tracked (lost) object, we provide a feature-descriptor storing mechanism for the tracked object in dif-



(a) Our custom-built quadrotor used in our field experiments.

(b) Text query: a drone. Goal: detect the drone.

(c) Text queries: (i) a whale in the water, and (ii) empty water. Goal: detect query (i).
 (d) Text query: a drone. Goal: detect the drone.

Fig. 7: **7(a): The used custom-built quadrotor in our experiments. 7(b)–7(d): Experimental results on automatic detection via text queries on low-resolution images.** In 7(b) the desired (correct) mask to detect is inside a larger mask, the cosine similarity between the query “a drone” to the smaller (correct) mask is less than the one between the same query to the larger mask. This is due to the image being lower in resolution, the small (correct) mask does not contain enough raw information, and thus detection refers to the big (larger/incorrect) mask. To solve this we remove the background mask as in Figure 7(d) (single query) and 7(c) (multiclass), however, in some cases, the row data from the cropped mask still does not provide enough data for CLIP.



Fig. 8: **Automatic detection experiments via text queries (SAM-and-Clip).** We tested different types of text-based detection including standard detection, scene reasoning-based detection, special attribute-based detection, special prior knowledge-based detection, and a combination of the last two.

ferent stages of the tracking process, these stored features, will be used to find the object once lost. Specifically, we suggest the following. Let $\tau > 0$ be an integer. During the tracking, at each iteration i such that $i\% \tau = 0$, define M_i^{obj} to be the mask denoting the current tracked object in the frame, we first apply Desc on the current frame F_i to obtain $D_i := \text{Desc}(F_i) \in \mathbb{R}^{h \times w \times d}$, then we compute the mean descriptor of the current tracked object as:

$$v_i^{obj} := \frac{1}{\text{non-zero}(M_i^{obj})} \sum_{p \in D_i[M_i^{obj}]} p$$

This feature represents the tracked object in the i th step. We thus store this descriptor and add it to the set of previously computed descriptors to obtain the set

$$V^{obj} := \{v_0^{obj}, v_\tau^{obj}, v_{2\tau}^{obj}, \dots, v_i^{obj}\}$$

Now, whenever the system loses the tracked object, we apply the following recovery mechanism. The system goes back to the detection stage, with a query feature descriptor

at hand as

$$v = \frac{1}{|V^{obj}|} \sum_{v^{obj} \in V^{obj}} v^{obj},$$

seeking the closest region (if any) from the segmented frame, and thus re-detecting the object. Here, the segmentation might be given by the segmentation model (e.g., SAM), or by the tracker which tries to re-detect the lost object. Note we use the mean to gain faster performance for real-time applications, however, other techniques can be used to improve the robustness.

III. EXPERIMENTS

We conducted several quadrotor experiments for zero-shot detection, tracking, and following different objects. First, we provide details about the system and its implementation.

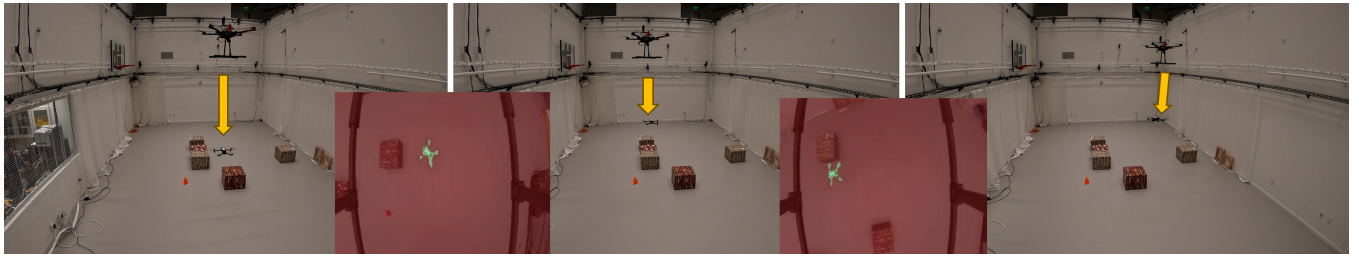
A. Hardware

We showcase the capability of our system using a quadrotor equipped with an RGB camera. The quadrotor is custom-built with a Pixhawk running PX4 flight control software. The camera data is streamed directly to a remote ground station computer (equipped with an NVIDIA GeForce RTX 2070) using the “herelink” digital transmission system along with other telemetry data. The ground station runs the tracking algorithm and sends control commands to the quadrotor via Mavlink. To enable indoor testing, the quadrotor is also equipped with an onboard computer that runs MAVROS and interfaces with an external Vicon motion capture system to get the position. The quadrotor is shown in Figure 7(a).

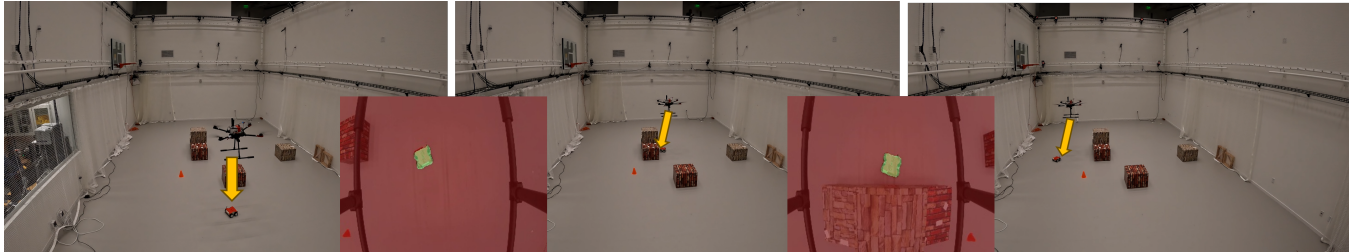
B. Implementation, System Details, and Setup

While code (system) implementations are sometimes overlooked and seen as “technical details”, we argue that it is crucial for designing our *FAn* system with top real-time (highly applicable) performance, thus, we now provide the main details with respect to our system.

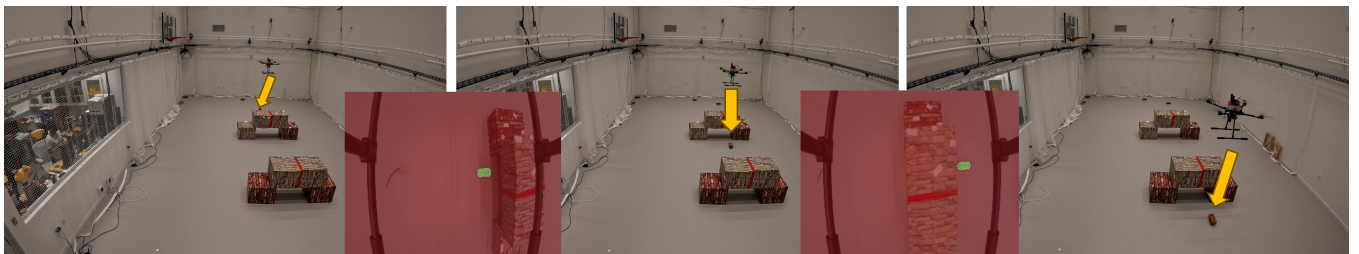
Real-time operating. Real-time object detection and following require processing large amounts of data quickly. To do so, we compress SAM and DINO via quantization and



(a) Drone following a drone



(b) Drone following a toy car



(c) Drone following a toy (manually moved) brick

Fig. 9: **Experimental results on automatic tracking, following, and re-detection.** The tracked object is referred to by the yellow arrow, we also show the results of the re-detection mechanism in the last two rows.

tracking to improve the running time of the segmentation and detection step. We also use FastSAM to improve computation speed. As for the tracking step, we also support the usage of SiamMask [30] tracker which is known to be fast, specifically for single object tracking; see Table I which reports the runtime (FPS) for every model used in our work.

Flight controller. To be highly applicable as possible, we used PX4, an open-source flight control software, to communicate with our quadrotor. PX4 provides a flexible and customizable platform for controlling unmanned vehicles, we thus use it to send control commands to the drone. Specifically, we use the MAVSDK Python library to send velocity commands to the drone, which allows us to control its 3D translational velocities and its yaw rate. Since MAVSDK is an open-source library that provides easy-to-use APIs for communicating with PX4-based drones, enabling quick and easy integration of our system into future projects.

Visual servoing. In our experiments, the onboard camera is mounted on the bottom of the quadrotor facing the ground. At relatively small translational velocities the first-order approximations of roll and pitch angles are close to zero. In addition, we fix the drone altitude and yaw angle throughout each experiment. Under these assumptions, the visual servoing task comes down to tracking a coordinate

in the 2D plane via translational velocity commands. We opt for a proportional controller for our indoor experiments: taking pixel distance between the center of mass of the object of interest and the center pixel along both the X and Y directions in the input frame to generate proportionate forward/backward and left/right quadrotor velocities. Also, to achieve smooth quadrotor trajectories while following an object, *FAn* preprocesses the input signal using a lowpass filter on the pixel positions of the tracked object. The filter reduces any high-frequency jittering that could arise from the tracking algorithm in challenging visual scenes or from an object's erratic movement. This ensures that the drone moves smoothly and avoids jerky actions that invalidate the small roll and pitch assumptions and can affect tracking accuracy. The combination of the lowpass preprocessing of the input signal with a propositional velocity controller along with the other components of the *FAn* system is sufficient to achieve smooth, accurate, and efficient object tracking and following by the quadrotor at speeds considered for indoor testing.

Video Streaming. In our system, it is necessary to process frames from an online video stream in real-time continuously. To achieve this we implemented an online streamer using the OpenCV library in Python. To ensure low latency, we execute a thread that is continuously reading frames from

the video stream using the ‘cv2.read()’ command, allowing us to keep processing the latest available frames without any significant delay. To make sure that we always have access to the latest frame, we set the buffer size of the OpenCV read stream to 1. To retrieve the latest frame from our online streamer, we simply call a method that returns the last frame that was read by the thread. This ensures that the system always has access to the most recent frame when it needs it.

C. Results.

We test the proposed *FAn* system on multimodal detecting, tracking, re-detecting, and following different objects.

Zero shot detection results with SAM and DINO. We experiment with our zero-shot detection technique on various objects. Figure 4 and Figure 2 show example results for real-time detection via SAM+DINO, where the provided queries are clicks on the desired objects from other pictures (We also provide a script for obtaining these click queries). One can see that the detection works well for both high and low-resolution images, where SAM provides good regions, DINO accurately classifies each region to the correct label, and thus the detection is applied properly. Explanations regarding correct DINO classifications are provided in Figure 3, where we plot heatmaps with respect to cosine similarity computed between every pixel DINO feature descriptor and some focal point pixel. One can see that pixels with similar semantics are very similar to each other in terms of DINO features.

Zero shot detection results using solely fast DINO. In Figure 5 we have several examples showcasing the efficiency of our rapid automated detection system on (1) whales, (2) drones, (3) RC cars, and (4) bricks. While this approach is significantly faster and performs admirably with objects possessing distinct shapes such as drones and whales, it yields less precise segmentation, increasing the likelihood of missed detections, particularly for objects lacking unique shapes like the brick in the last column.

Zero shot detection results with SAM and CLIP. We also experiment with real-time detection via “text” prompts via SAM+CLIP. For high-resolution images, the reasoning and detection are robust. We conduct the following 4 tests: (i) **Standard detection**, e.g., “detect a whale”, (ii) **scene reasoning-based detection**, where such tasks require a good understanding of the scene, for example, “detect the boy holding the ball”.(iii) **Special attribute-based detection**, here, we seek objects with specific attributes, like, “detect the white dog”. (iv) **Special prior knowledge-based detection**. In this case, the system should have prior knowledge of a specific object like its name/nickname. For example “detect Messi/Cristiano Ronaldo”. (v) **Special prior knowledge& attribute based detection**. A mix of the previous two cases, e.g., “detect a Real Madrid player”. In Figure 8 we report the results of this experiment.

However, for low-resolution images, SAM+CLIP detections are not as robust. This occurs specifically when the desired mask to detect is placed inside a larger mask, and thus, the detection refers to the larger mask instead of the smaller (correct) one. As the image has low resolution, the

small (correct) mask does not present enough raw information, and is thus misclassified. Figure 7 shows an example of low-resolution images for such scenarios.

Real time any object following tests. We tested our overall system on the following RC cars, drones, and bricks in real-time. We also demonstrate our system **for re-detecting** an object that gets occluded from the scene during tracking. Specifically, during the following experiments, the RC car and the brick, where they pass under a “tunnel” twice, and our proposed re-detection mechanism is able to recover and resume tracking. Figures 9(a), 9(b), and 9(c) show different scenarios during the following. We encourage the reader to view the demos on our [project webpage](#) and in the [explainer video](#).

IV. CONCLUSIONS

FAn is a comprehensive system that bridges the gap between SOTA computer vision and robotic systems, providing an end-to-end solution for segmenting, detecting, tracking, and following any object. Its open set, multimodal, real-time capabilities, adaptability to different environments, and open-source code make it a valuable tool for a wide range of industries and applications.

REFERENCES

- [1] A. Radford, J. W. Kim, C. Hallacy, A. Ramesh, G. Goh, S. Agarwal, G. Sastry, A. Askell, P. Mishkin, J. Clark *et al.*, “Learning transferable visual models from natural language supervision,” in *International conference on machine learning*. PMLR, 2021, pp. 8748–8763. 1, 2, 3
- [2] M. Caron, H. Touvron, I. Misra, H. Jégou, J. Mairal, P. Bojanowski, and A. Joulin, “Emerging properties in self-supervised vision transformers,” in *Proceedings of the IEEE/CVF international conference on computer vision*, 2021, pp. 9650–9660. 1, 2, 3
- [3] A. Kirillov, E. Mintun, N. Ravi, H. Mao, C. Rolland, L. Gustafson, T. Xiao, S. Whitehead, A. C. Berg, W.-Y. Lo *et al.*, “Segment anything,” *arXiv preprint arXiv:2304.02643*, 2023. 1, 3
- [4] B. Taha and A. Shoufan, “Machine learning-based drone detection and classification: State-of-the-art in research,” *IEEE Access*, vol. 7, pp. 138 669–138 682, 2019. 1
- [5] A. Maalouf, Y. Gurfinkel, B. Diker, O. Gal, D. Rus, and D. Feldman, “Deep learning on home drone: Searching for the optimal architecture,” *arXiv preprint arXiv:2209.11064*, 2022. 1
- [6] H. Naeem, J. Ahmad, and M. Tayyab, “Real-time object detection and tracking,” *INMIC*, pp. 148–153, 2013. 1
- [7] A. Koubãa and B. Qureshi, “Dronetrack: Cloud-based real-time object tracking using unmanned aerial vehicles over the internet,” *IEEE Access*, vol. 6, pp. 13 810–13 824, 2018. 1
- [8] Z. Chen, R. Khemmar, B. Decoux, A. Atahouet, and J.-Y. Ertaud, “Real time object detection, tracking, and distance and motion estimation based on deep learning: Application to smart mobility,” in *2019 Eighth International Conference on Emerging Security Technologies (EST)*. IEEE, 2019, pp. 1–6. 1
- [9] A. Restas *et al.*, “Drone applications for supporting disaster management,” *World Journal of Engineering and Technology*, vol. 3, no. 03, p. 316, 2015. 1
- [10] D. Tezza and M. Andujar, “The state-of-the-art of human–drone interaction: A survey,” *IEEE Access*, vol. 7, pp. 167 438–167 454, 2019. 1
- [11] P. Nousi, I. Mademlis, I. Karakostas, A. Tefas, and I. Pitas, “Embedded uav real-time visual object detection and tracking,” in *2019 IEEE International Conference on Real-time Computing and Robotics (RCAR)*, 2019, pp. 708–713. 1
- [12] J. Zhao, J. Zhang, D. Li, and D. Wang, “Vision-based anti-uav detection and tracking,” *IEEE Transactions on Intelligent Transportation Systems*, vol. 23, no. 12, pp. 25 323–25 334, 2022. 1

- [13] S. R. Ganti and Y. Kim, "Implementation of detection and tracking mechanism for small uas," in *2016 International Conference on Unmanned Aircraft Systems (ICUAS)*. IEEE, 2016, pp. 1254–1260. [1](#)
- [14] E. Unlu, E. Zenou, N. Riviere, and P.-E. Dupouy, "Deep learning-based strategies for the detection and tracking of drones using several cameras," *IPSA Transactions on Computer Vision and Applications*, vol. 11, no. 1, pp. 1–13, 2019. [1](#)
- [15] R. Barták and A. Vykovský, "Any object tracking and following by a flying drone," in *2015 Fourteenth Mexican International Conference on Artificial Intelligence (MICAI)*, 2015, pp. 35–41. [1](#)
- [16] A. Barisic, M. Car, and S. Bogdan, "Vision-based system for a real-time detection and following of uav," in *2019 Workshop on Research, Education and Development of Unmanned Aerial Systems (RED UAS)*, 2019, pp. 156–159. [1](#)
- [17] C. Jia, Y. Yang, Y. Xia, Y.-T. Chen, Z. Parekh, H. Pham, Q. Le, Y.-H. Sung, Z. Li, and T. Duerig, "Scaling up visual and vision-language representation learning with noisy text supervision," in *International conference on machine learning*. PMLR, 2021, pp. 4904–4916. [2](#)
- [18] A. Guzhov, F. Raue, J. Hees, and A. Dengel, "Audioclip: Extending clip to image, text and audio," in *ICASSP 2022-2022 IEEE International Conference on Acoustics, Speech and Signal Processing (ICASSP)*. IEEE, 2022, pp. 976–980. [2](#)
- [19] S. Tellex, N. Gopalan, H. Kress-Gazit, and C. Matuszek, "Robots that use language," *Annual Review of Control, Robotics, and Autonomous Systems*, vol. 3, pp. 25–55, 2020. [2](#)
- [20] Y. Bisk, A. Holtzman, J. Thomason, J. Andreas, Y. Bengio, J. Chai, M. Lapata, A. Lazaridou, J. May, A. Nisnevich *et al.*, "Experience grounds language," *arXiv preprint arXiv:2004.10151*, 2020. [2](#)
- [21] M. Ahn, A. Brohan, N. Brown, Y. Chebotar, O. Cortes, B. David, C. Finn, C. Fu, K. Gopalakrishnan, K. Hausman *et al.*, "Do as i can, not as i say: Grounding language in robotic affordances," *arXiv preprint arXiv:2204.01691*, 2022. [2](#)
- [22] A. Brohan, N. Brown, J. Carbajal, Y. Chebotar, J. Dabis, C. Finn, K. Gopalakrishnan, K. Hausman, A. Herzog, J. Hsu *et al.*, "Rt-1: Robotics transformer for real-world control at scale," *arXiv preprint arXiv:2212.06817*, 2022. [2](#)
- [23] S. Li, X. Puig, C. Paxton, Y. Du, C. Wang, L. Fan, T. Chen, D.-A. Huang, E. Akyürek, A. Anandkumar *et al.*, "Pre-trained language models for interactive decision-making," *Advances in Neural Information Processing Systems*, vol. 35, pp. 31 199–31 212, 2022. [2](#)
- [24] A. Ramesh, M. Pavlov, G. Goh, S. Gray, C. Voss, A. Radford, M. Chen, and I. Sutskever, "Zero-shot text-to-image generation," in *International Conference on Machine Learning*. PMLR, 2021, pp. 8821–8831. [2](#)
- [25] K. Crowson, S. Biderman, D. Kornis, D. Stander, E. Hallahan, L. Castrioto, and E. Raff, "Vqgan-clip: Open domain image generation and editing with natural language guidance," in *European Conference on Computer Vision*. Springer, 2022, pp. 88–105. [2](#)
- [26] O. Patashnik, Z. Wu, E. Shechtman, D. Cohen-Or, and D. Lischinski, "Styleclip: Text-driven manipulation of stylegan imagery," in *Proceedings of the IEEE/CVF International Conference on Computer Vision*, 2021, pp. 2085–2094. [2](#)
- [27] A. Ramesh, P. Dhariwal, A. Nichol, C. Chu, and M. Chen, "Hierarchical text-conditional image generation with clip latents," *arXiv preprint arXiv:2204.06125*, 2022. [2](#)
- [28] Z. Yang and Y. Yang, "Decoupling features in hierarchical propagation for video object segmentation," in *Advances in Neural Information Processing Systems (NeurIPS)*, 2022. [3](#)
- [29] Z. Yang, J. Miao, X. Wang, Y. Wei, and Y. Yang, "Scalable multi-object identification for video object segmentation," *arXiv preprint arXiv:2203.11442*, 2022. [3](#)
- [30] Q. Wang, L. Zhang, L. Bertinetto, W. Hu, and P. H. Torr, "Fast online object tracking and segmentation: A unifying approach," in *Proceedings of the IEEE conference on computer vision and pattern recognition*, 2019. [3](#), [7](#)
- [31] B. Cheng, I. Misra, A. G. Schwing, A. Kirillov, and R. Girdhar, "Masked-attention mask transformer for universal image segmentation," in *Proceedings of the IEEE/CVF Conference on Computer Vision and Pattern Recognition*, 2022, pp. 1290–1299. [3](#)
- [32] S. Amir, Y. Gandelman, S. Bagon, and T. Dekel, "Deep vit features as dense visual descriptors," *arXiv preprint arXiv:2112.05814*, 2021. [3](#), [5](#)
- [33] K. M. Jatavallabhula, A. Kuwajerwala, Q. Gu, M. Omama, T. Chen, S. Li, G. Iyer, S. Saryazdi, N. Keetha, A. Tewari *et al.*, "Conceptfusion: Open-set multimodal 3d mapping," *arXiv preprint arXiv:2302.07241*, 2023. [3](#), [5](#)
- [34] X. Zhao, W. Ding, Y. An, Y. Du, T. Yu, M. Li, M. Tang, and J. Wang, "Fast segment anything," 2023. [4](#)
- [35] S. Liu, Z. Zeng, T. Ren, F. Li, H. Zhang, J. Yang, C. Li, J. Yang, H. Su, J. Zhu *et al.*, "Grounding dino: Marrying dino with grounded pre-training for open-set object detection," *arXiv preprint arXiv:2303.05499*, 2023. [5](#)
- [36] B. Li, K. Q. Weinberger, S. Belongie, V. Koltun, and R. Ranftl, "Language-driven semantic segmentation," *arXiv preprint arXiv:2201.03546*, 2022. [5](#)
- [37] H. Zhao, X. Puig, B. Zhou, S. Fidler, and A. Torralba, "Open vocabulary scene parsing," in *Proceedings of the IEEE International Conference on Computer Vision*, 2017, pp. 2002–2010. [5](#)
- [38] G. Ghiasi, X. Gu, Y. Cui, and T.-Y. Lin, "Scaling open-vocabulary image segmentation with image-level labels," in *Computer Vision—ECCV 2022: 17th European Conference, Tel Aviv, Israel, October 23–27, 2022, Proceedings, Part XXXVI*. Springer, 2022, pp. 540–557. [5](#)
- [39] Y. Zhong, J. Yang, P. Zhang, C. Li, N. Codella, L. H. Li, L. Zhou, X. Dai, L. Yuan, Y. Li *et al.*, "Regionclip: Region-based language-image pretraining," in *Proceedings of the IEEE/CVF Conference on Computer Vision and Pattern Recognition*, 2022, pp. 16 793–16 803. [5](#)